Demonstration of Multi-casting in a 1×9 LCOS Wavelength Selective Switch

Brian Robertson[1], Haining Yang[1], Maura M. Redmond[1], Neil Collings[1], John R. Moore[1], Jinsong Liu[1], Anna M. Jeziorska-Chapman[1], Mike Pivnenko[1], Sharon Lee[2], Adrian Wonfor[2], Ian H. White[2], William A. Crossland[1], and D. P. Chu[1*]

Abstract— **A multi-functional 1×9 wavelength selective switch based on liquid crystal on silicon (LCOS) spatial light modulator technology and anamorphic optics was tested at a channel spacing of 100 GHz and 200 GHz, including dynamic data measurements on both single beam deflection and multi-casting to two ports. The multi-casting holograms were optimized using a modified Gerchberg-Saxton routine to design the core hologram, followed by a simulated annealing routine to reduce crosstalk at non-switched ports. The effect of clamping the magnitude of phase changes between neighboring pixels during optimization was investigated, with experimental results for multi-casting to two ports resulting in a signal insertion loss of -7.6 dB normalized to single port deflection, a uniformity of ±0.6 %, and a worst case crosstalk of -19.4 dB, which can all be improved further by using a better anti-reflection coating on the LCOS SLM coverplate and other measures.**

***Index Terms*—Multi-casting, optical fiber communication, wavelength division multiplexing, wavelength selective switch**

I. Introduction

One of the key components in current and next generation wavelength de-multiplexing (WDM) reconfigurable optical add-drop multiplexers (ROADMs) are 1×N wavelength selective switches (WSSs) [1, 2]. Currently there are two main competing technologies; micro electromechanical systems (MEMSs) [3, 4], and liquid crystal on silicon (LCOS) spatial light modulator (SLM) switches [5, 6]. Both are used commercially. However, LCOS based WSSs have several advantages, including flexible spectrum coverage [7], adaptive alignment [8], and robustness. In this paper we demonstrate a 1×9 WSS based on LCOS technology and anamorphic optics that is capable of deflecting a signal to multiple output ports, an operation referred to as multi-casting. This functionality is advantageous as we can potentially balance power in a ROADM switching node by deflecting excess light away from the signal ports whilst also increasing architectural flexibility. Furthermore, the low cost and robust nature of our design makes it possible to push the technology towards the customer end: at street corners or even the household in the next decade.

Manuscript received June 1, 2013.

[1]Photonics and Sensors Group, Department of Engineering, University of Cambridge, 9 JJ Thomson Avenue, CB3 0FA, Cambridge, UK

[2]Photonics Systems Group, Department of Engineering, University of Cambridge, 9 JJ Thomson Avenue, CB3 0FA, Cambridge, UK

[*]Corresponding author: dpc31@cam.ac.uk

A range of multi-casting hologram design techniques for LCOS SLMs have been previously developed, including algorithms based on simulated annealing (SA) [9], direct binary search [10], and variants of the Gerchberg-Saxton (GS) algorithm [11]. Multi-casting in a LCOS WSS to two ports has been previously reported by Frisken et al [12], where light was split by adding a square phase modulation of π to a linear phase ramp. In addition, Schröder et al [13] recently reported the design of holograms capable of multi-casting to four output positions for use in an optical processing system based on a LCOS WSS. Our research differs in that we are investigating arbitrary, equal weighted fan-out holograms for use in a nine port WSS with the aim of minimizing signal non-uniformity and suppressing the crosstalk to < -40 dB. To design the hologram we use a hybrid optimization routine. In the first step a non-standard Gerchberg-Saxton (GS) algorithm, termed a ray-trace based GS algorithm [14], generates the initial phase pattern. In the second step we apply simulated annealing (SA) to minimize crosstalk at specific regions of the replay field, whilst maintaining signal integrity.

Hybrid optimization algorithms have been previously developed [15, 16]. For example Fan et al. [15] et al used a Gerchberg-Saxton algorithm followed by a genetic algorithm step to design a 1×6 fan-out hologram. The first GS stage was used to generate a set of initial phase patterns which were then by the genetic algorithm to optimize the final hologram. In our approach the ray-trace based GS algorithm calculates a single starting hologram, which is then optimized by the SA step based on a merit function with terms for efficiency, non-uniformity, and crosstalk.

We discuss two considerations during optimization. Firstly, as lenslet arrays are used to couple the fiber array to the switch, we describe an algorithm that suppresses crosstalk across regions of the replay field corresponding to the beam diameter at the lenslet facets, as opposed to discrete locations. All possible equal weighting multi-casting patterns are optimized and analyzed. Secondly, we analyze the effect that clamping the magnitude of the phase change between adjacent pixels during the SA optimization in order to investigate whether large phase discontinuities have an effect on multi-casting performance. As far as we are aware, this is the first time that such hybrid algorithm based on a ray-trace based GS algorithm in conjunction with a SA optimization algorithm has been theoretically and experimentally investigated in a LCOS based WSS.

In this paper we first outline the design of a 1×9 WSS, and then detail the algorithm used to design the multi-casting holograms. We then report and discuss the theoretical performance for all possible fan-out configurations having equal fan-out weighting designed using our two-step algorithm. The static performance of the switch for single port deflections at 100 GHz channel spacing is presented, along with data taken during dynamic data tests at 10 Gbit/s. Finally, the static and dynamic performance when multi-casting equal power to two output ports is given.

II. Design of Wavelength Selective Switch

A. LCOS SLM

A LCOS SLM is a pixelated reflective device that can display a quantized, reconfigurable phase-only hologram. The SLM used in this work consists of an array of 1280×720 pixels on a pitch of Δ = 15 µm, and employs an analogue voltage drive scheme. The inter-pixel gap, g, has a value of 0.46 µm, giving a fill factor of $\rho = ((\Delta-g)/\Delta)^2 = 0.94$. A nematic liquid crystal (BLO37 as purchased from Merck) is used, and the SLM is capable of resolving 256 discrete phase levels with a maximum modulation of 2.2π at 1550 nm. Assembly of the device was carried out in-house [17], and an anti-reflection coated substrate (reflectivity of 0.2 %) was index matched to the front cover glass of the SLM.

B. Optical Design

Figures 1(a) and (b) show the layout of the switch, which consists of a 1×12 single mode fiber ribbon on a δ = 250 µm pitch, a lenslet array (L_A), a collimating lens (L_1), a transmission grating (G_S), a cylindrical lens (L_2), and a nematic LCOS SLM. The input WDM signals are launched into the switch via port 6 (IN). The refractive lenslet array converts the 5.2 µm input fiber Gaussian beam waist to a larger radius waist of w_1 that that better matches the dimensions of the optical components and the deflection capabilities of the SLM [18]. As the system is folded by G_S, we define two coordinate systems; xyz aligned to the LCOS SLM, and x′y′z′ aligned to the fiber array.

The signal beam is collimated by L_1 (focal length f_1), and is then incident on the transmission grating, G_S, where the individual WDM wavelengths are angularly de-multiplexed. These beams are focused down by cylindrical lens L_2 (focal length f_2) onto the SLM to form a series of elliptical beams spaced by a distance of N_s pixels. Each area of the SLM covered by a beam is configured to operate as an independent sub-hologram of pixel dimensions $N_x \times N_y$. To minimize the effects of sub-hologram beam clipping on switch performance we set the limits that $N_y\Delta = 3w_y$, where w_x and w_y are respectively the Gaussian beam radii in the x and y-directions.

As shown in Fig. 2(b), the switch operates as a Fourier-transform system in the y-direction, with the plane P_1 placed at the front focal plane of lens L_1, and the SLM placed at the back focal plane. In the x-direction there is an imaging condition between the SLM fiber output planes (Fig. 2(a)). Thus the sub-hologram can only deflect in the yz plane [19], although optimizing in the x-direction can control dispersion [20].

We designed the switch optics around a transmission grating that has a maximum polarization dependent loss (PDL) of < 0.25 dB, and an efficiency of >85 % across the C-band [21]. To make the switch fully polarization independent we must use a polarization insensitive SLM, based on, for example, an integrated quarter waveplate (QWP) [22] or a blue phase liquid crystal [23]. In the case of a switch employing an SLM with integrated QWP, the PDL of the intrinsic switch optics would be compensated for (overall PDL = 0), whilst in the case of a blue phase based SLM (SLM induces equal polarization component delay), the PDL of the overall intrinsic switch optics would be <0.5 dB, correctable using a selectively attenuating polarization filter. It should also be noted that higher performance transmission gratings (efficiency > 94 %, and a PDL of < 0.2 dB) are now commercially available [21]. However, during our experimental work, a polarization sensitive nematic SLM was used instead of the polarization insensitive SLMs described above. Thus, the input polarization state had to be controlled to minimize insertion loss.

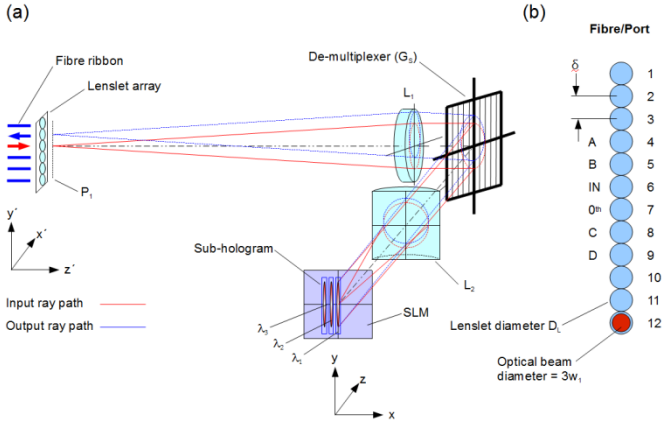

Fig. 1 Schematic diagram of the switch showing associated port assignments.

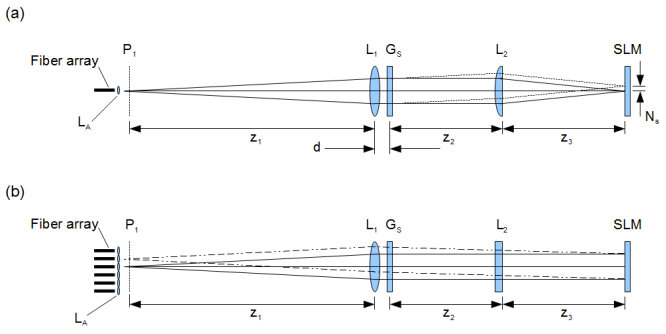

Fig. 2 *Layout of the test-switch optics (unfolded). (a) View in xz-plane showing light being de-multiplexed. (b) View in yz-plane showing light deflected by SLM.*

The input fiber (port 6) is offset from the optical axis by a distance $y' = -\delta/2$. As a result, if no grating is displayed, the light retraces its path, is re-multiplexed by G_S, and is focused at port 7 a distance $\delta/2$ above the optical axis (0^{th} order position). By displaying a phase grating of period T_n on the n^{th} sub-hologram (wavelength λ_n), the light is diffracted in the yz plane through an angle of θ_n with respect to the z-axis given

by the grating equation. This beam is focused down by L_1 at plane P_1, at position y'_n, = $f_1\tan\theta_n$.

To minimize roll-off in insertion loss with beam steering angle, we must ensure the system of Fig. 2 is telecentric in the plane of deflection ($z_1 = f_1$ and $z_2+z_3 = f_1$). A second condition applies to the cylindrical lens, in that the static grating, G_S, must be placed at its front focal plane, and the SLM at its back focal plane ($z_2 = f_2$, and $z_3 = f_2$). If this were not the case, the beams would be focused at an angle to the fiber optical axis, with the angle increasing with $|y'_n|$. As a result we must also ensure that $f_1 = 2f_2$, and for optimum performance, the separation d, between L_1 and G_S must be minimized (see Fig. 2(a)). We use off-the-shelf optomechanics, with d~20 mm. However, this does not affect system performance significantly over the range of wavelengths tested.

The de-multiplexing grating, G_S, has a spatial frequency of 940.07 lines/mm and is designed to operate at a Littrow angle of 46.5º. Thus at the central C-band wavelength the dispersion angle is $\Delta\theta_d = 0.0623$º, and $\theta_{+1} = 46.5$° [21]. This dispersion angle is related to the sub-hologram pixel pitch, N_s, by

$$N_s = f_2 \tan(\theta_d)/\Delta \qquad (1)$$

The ratio $Q = N_s/N_x$ determines the passband of the optical switch; the smaller the value of Q, the greater the passband [24]. For 100 GHz operation it was decided to set $N_x = 5$ and $N_s = 7$ (Q = 1.4), giving a gap of one pixel between the sub-holograms. Thus, as $\Delta = 15$ μm, we set $w_x = N_x\Delta/3 = 25$ μm, giving $f_2 = 96.56$ mm (from Eq. (1)). We chose the nearest off-the-shelf achromat with $f_2 = 100$ mm, thereby setting $f_1 = 200$ mm. The major and minor Gaussian beam radii ($1/e^2$) at the SLM, w_y and w_x, are calculated through the application of Gaussian beam optics to Fig. 2, which gives $w_y = f_1\lambda/(\pi w_1)$ and $w_x = f_2 w_1/f1$. As a result $w_1 = 50$ μm, and $3w_y = 5.90$ mm ($N_y = 393$ pixels). A fused silica refractive lenslet array of focal length 743 μm is used to convert the 5.2μm input beam radius to our target value of 50 μm. It should be noted that to test the switch performance at an alternative channel spacing, such as 50 GHz or 200 GHz, the fiber/lenslet array separation must be adjusted to optimize w_1 and the x-beam radius at the SLM plane.

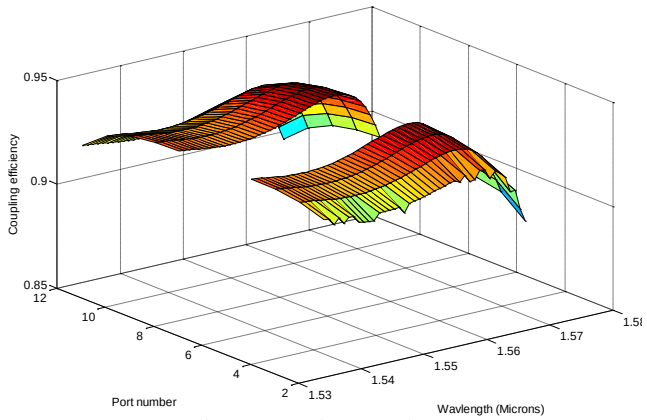

Fig. 3 *Fiber coupling efficiency as a function of C-band wavelength and port position*

TABLE I
OPTICAL POWER BUDGET

Component	Passes	Transmission (%)	Total Loss (dB)
Fiber facet	2	96	-0.35
Lenslet Array	2	99	-0.09
Collimating lens	2	99	-0.09
De-multiplexer	2	87.7	-1.14
Cylindrical lens	2	99	-0.09
SLM reflectivity	1	90.0	-0.46
Optical aberrations, η_A	1	91.9±2.4	-0.37±0.11
Diffraction efficiency, η_G	1	87.0±0.3	-0.61±0.02
Total loss			**-3.2±0.1**

Ideally, the deflection angle introduced at the SLM plane is preserved on passing back through G_s. However, as the signal beams are incident on the transmission grating out-of-plane, we observe conical diffraction [25], which leads to a lateral offset error in x_n', and thus an increase in insertion loss of the +1 order, with increasing y'_n.

The coupling efficiency at a specific λ and port position, N, denoted by η(N, λ), is the product of the fixed system loss, η_f, the loss due to optical aberrations, η_A, and the theoretical grating diffraction efficiency roll-off as a function of port position, η_G. This can be expressed as:

$$\eta(N,\lambda) = \eta_f \eta_A(N,\lambda)\eta_G(N,\lambda) \qquad (2)$$

The theoretical fiber coupling efficiency, η_A, as a function of C-band wavelength and port position is illustrated in Fig. 3. This is calculated using the ray-tracing package Zemax [26], with the switch component positions optimized to ensure best average efficiency. As can be seen, $\eta_A = 91.9\pm2.4$ %, with an asymmetric wavelength roll-off due to a combination of optical aberrations and conical diffraction. A tolerance analysis of the switch shows that alignment errors exacerbate this roll-off in coupling efficiency as well as introducing an asymmetry roll-off with respect to port direction. To calculate the grating diffraction efficiency, η_G, we employ a model developed by Gil Leyva et al [27] that includes the effects of blazed grating spatial and phase quantization, and inter-pixel gap.

The resulting theoretical insertion loss of the switch is detailed in Table 1. This shows that, including fixed component losses, $\eta(N,\lambda) = -3.2\pm0.1$ dB. It should be stressed that in Table 1, the SLM reflectivity is the average measured value. For practical applications it may be necessary to take into account the asymmetric Fabry-Perot cavities formed between the front coverplate surface, ITO layer, and aluminum pixels during hologram optimization.

The intrinsic polarization dependent loss of the system optics was measured to be <0.6 dB when a dielectric mirror was positioned at the SLM plane. This is in good agreement with the predicted value of 0.5 dB.

C. Optimization of Multi-Casting Holograms

As mentioned, the anamorphic switch optics performs a Fourier-transform in the y′ direction only [19]. Thus, the intensity distribution in the output plane, $I_R(x', y')$, is given by

$$I_R(x',y') = \left| FT\left[\exp\left[-\frac{y^2}{w_y^2} \right] \exp\left(i\varphi_R(y)\right) \right] \right|^2 \times \exp\left[-2x'^2 / w_1^2 \right] \quad (3)$$

Here $\varphi_H(y)$ is the hologram phase profile, w_y is the Gaussian beam radius in the y direction at the sub-hologram, and FT denotes a one-dimensional Fourier transform. For this work we use a two-stage algorithm for the hologram design: a modified GS optimization with a ray-trace calculation to set up the initial phase pattern [14], and SA to suppress crosstalk at the non-switched output ports (target <-40 dB). This will be referred to as the GSSA algorithm. As can be seen from Eq. (3), design of the hologram can be reduced to the one-dimensional problem of optimizing $\varphi_H(y)$. Note that Eq. (3) neglects the effect of conical diffraction by the transmission grating.

In this paper we focus on setting up a suitable merit function and boundary conditions for the hologram optimization. Best results are obtained when the merit function minimizes crosstalk across specific regions of the output field (approximately $2w_1$ beam width at the output lenslets). Let us assume we wish to deflect to N_{max} output ports with a fan-out of F, and with a weighting of β_N at each port. We define the (N_{max}-F) segments of the replay field where crosstalk is minimized as suppression windows, with a width of p_w. The merit function, *MF*, is defined by setting the peak values at positions where there is a signal as $\beta_N I_o$, where I_o is the peak intensity, and across the suppression windows we set the intensity as zero. Thus

$$MF = \gamma_s \sum_{N=signal} abs\left|\left(\beta_N I_o - I(y'_N)\right)\right| + \gamma_{ns} \sum_{N\neq signal} \int_{y'_N - p_w/2}^{y'_N - p_w/2} I(y')dx' + \gamma_u \sum_{N=signal} \sum_{K=signal} \left|\left(I(y'_N) - I(y'_K)\right)\right| c_{NK} \quad (4)$$

where γ_s and γ_{ns} are weightings of the terms, adjusted to ensure convergence. A third term with weighting γ_u is added to maximize signal balance, allowing us to optimize with respect to either uniformity or efficiency. This term sums the relative difference between signal powers at positions N and K with a pre-defined weighting of c_{NK} for maximum flexibility.

For each iteration of the simulated annealing stage, the algorithm restricts the maximum phase change of a pixel with respect to neighboring pixels to φ_{LIMIT}. This is because we believe that due to the edge effect associated with LCOS devices, large phase discontinuities will not be displayed properly [28, 29]. Thus we wish to minimize as much as possible additional phase jumps in the final GSSA designed hologram. Finally, although the power coupled into the output fibers by the resultant hologram is calculated via a mode overlap integral between the Gaussian mode at plane P_1 and the replay field $E_R(x', y')$ [29], during optimization, the merit function used just the intensity distribution at the replay field (Eq. 4). This was in order to minimize the calculation time for the full hologram set.

In Fig. 4(a) we plot $I_R(x', y')$ at $x' = 0$ for an example hologram, where we deflect equal power to ports 2 and 3 whilst suppressing power to the other seven signal ports (ports 3-5 and 8-12). Note that as light diffracted outside these port positions is not important in terms of switch uniformity and crosstalk, no limits on the optical intensity in these regions were imposed during optimization. This is also true for the replay intensity at ports 6 and 7. Thus, the intensity levels (noise) can exceed our target value of -40 dB in these areas.

Ideally the theoretical insertion loss should be -3 dB to each port (50/50 split). The solid curve in Fig. 4(a) shows the intensity profile after applying the GS algorithm with ten optimization steps, and the dashed curve the intensity profile for the GSSA algorithm with twenty SA iterations, $\varphi_{LIMIT} = 1$ radian, and a value for $p_w = 100$ µm. For this particular example, the weighting factors for the GSSA merit function (Eq. 4) are set at $\gamma_s = 1$, $\gamma_{ns} = 10000$, and $\gamma_u = 5$. The holograms are optimized for replay at 1554.14 nm with 64 phase levels uniformly spaced between 0 and 2π, resulting in a minimum phase resolution of $\pi/32$ radians. These ideal phase levels are then rounded to the nearest available phase value of the LCOS SLM described in section 2.1 to match experimental conditions.

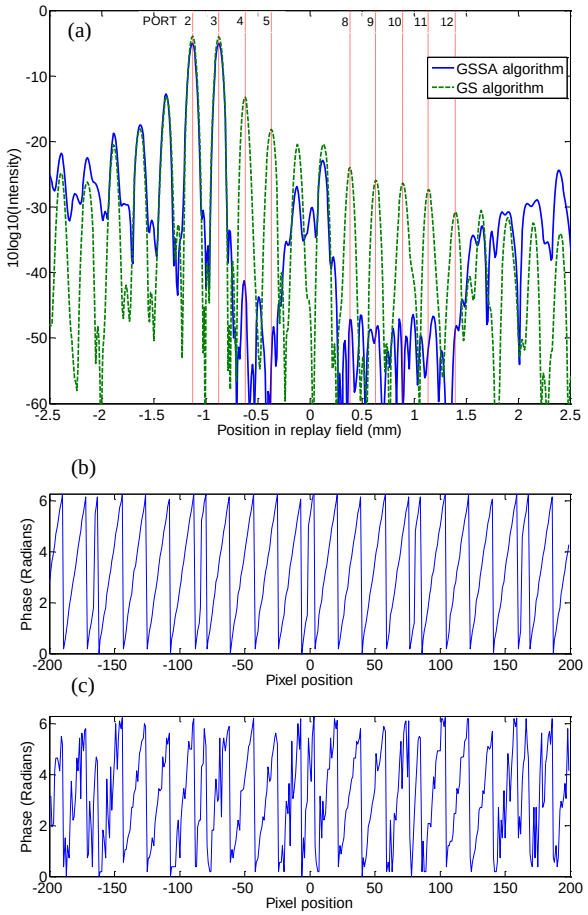

Fig. 4 *Theoretical replay field when sending equal power to ports 2 and 3. (a) Theoretical replay field for GS and GSSA algorithms. Dashed lines show port positions. (b) Optimized GS hologram phase profile. (c) Optimized GSSA hologram phase profile.*

The hologram optimization using the GS algorithm has a signal port insertion loss of –3.96 dB (normalized to the power

diffracted to a single port by an ideal blazed grating), a signal uniformity of <0.1 %, and a worst case crosstalk of -9.2 dB. However, as shown in Fig. 4(a), it is possible to suppress crosstalk effectively at the unused signal ports to <-40 dB target value whilst maintaining uniformity and efficiency using the GSSA algorithm. Theoretically, our ideal optimized hologram has an insertion loss of -4.96 dB, a worst case crosstalk of -44.6 dB, and a signal uniformity of U = ±0.6 %. For this specific example we define $U = (I_{N=3} - I_{N=2})/(I_{N=3} + I_{N=2})$. When this hologram is quantized to match the nearest available characterized LCOS SLM phase levels, the insertion loss is effectively unchanged at -4.95 dB, but the uniformity and worst case crosstalk increase slightly to ±0.7 % and -39.3 dB respectively. The hologram profiles for the GS and GSSA algorithms are shown in Figs. 4(b) and 4(c). As can be seen, the hologram optimized by the GSSA algorithm has essentially the same profile as that generated by the ray-traced GS algorithm. However, even though we apply a 1 radian limit on phase change between successive steps, there are still a few neighboring pixels changes where the eventual phase change exceeds this value.

In the case of N_{max} output fibers, there are a total of $(2^{N_{max}} - N_{max} - 1)$ configurations where the fan-out, F, is two or greater, and each signal channel has the same power. Thus, in order to fully test our GSSA algorithm, a set of 502 holograms were designed and analyzed covering all possible fan-out configurations. The performance of this hologram set is summarized in Table 2 as a function of F. The term H represents how many of the 502 optimized holograms have a fan-out of F. The average insertion loss was calculated by averaging the signal insertion loss of all F signals across all H holograms. The maximum non-uniformity and minimum Signal-to-Crosstalk Ratio (SXR) are the worst case values across all H holograms, whilst the minimum and maximum diffraction efficiency indicates how much of the incident light is diffracted into the F signal beams for the worst and best-case holograms.

TABLE 2
THEORETICAL FAN-OUT PERFORMANCE

Fan-out	H	Average Insertion Loss (dB)	Max non-uniformity (%)	Min Eff (%)	Max Eff (%)	Minimum SXR (dB)
2	9	-5.2	0.3	43.9	75.7	37.8
3	36	-6.8	2.7	45.9	80.1	37.9
4	84	-8.0	1.5	43.2	84.2	37.3
5	126	-9.3	1.2	42.5	75.5	35.7
6	126	-9.7	1.1	54.1	75.1	37.7
7	84	-10.3	1.3	57.9	73.3	38.5
8	36	-10.8	1.0	62.4	62.4	39.4
9	9	-11.7	1.2	60.9	60.9	∞

For this calculation, the weighting factors for the GSSA merit function (Eq. 4) are set at $\gamma_s = 1$, $\gamma_{ns} = 5000$, and $\gamma_u = 5$, and $\varphi_{LIMIT} = 2\pi$ radians as simulations showed that these values give a good overall performance. From Table 2 it can be seen that the worst-case non-uniformity for each set of holograms is low, with a value < 3 % in all cases. The SXR, defined as the power coupled into a non-signal fiber with respect to the incident signal beam is approaching our target, in all cases being < 35 dB. However, there is a significant variation in diffraction efficiency between holograms with the same fan-out value. It was observed that as we reduce γ_{ns}, this variation in diffraction efficiency reduces, albeit at the expense of SXR and uniformity. Furthermore, analysis of the data showed that the absolute diffraction efficiency for a set fan-out value is pattern dependent. That is, if we re-optimize the holograms with the same parameters, the diffraction efficiency for a given fan-out pattern is essentially unchanged.

Figures 5(a) and (b) show typical simulated replay fields for arbitrary chosen holograms having a fan-out of four and six respectively. On investigation it was found that the first stage ray-trace GS algorithm produces core fan-out patterns with a diffraction efficiency > 80%, but with high crosstalk and non-uniformity. After applying the SA step, both the non-uniformity and SXR are controlled to acceptable values, albeit with significant variation in diffraction efficiency within a hologram sub-set. Thus, for a specific fan-out value, some form of power balancing would be required to keep the switch insertion loss at a fixed level for all holograms. This could potentially be achieved by routing a certain percentage of light in an unused direction. However, this would imply an increased loss in the switch as the signal powers would be balanced to the lowest efficiency fan-out pattern. In future work we plan to optimize the parameters in the merit function, and investigate the role that spatial and phase quantization has on multi-casting performance.

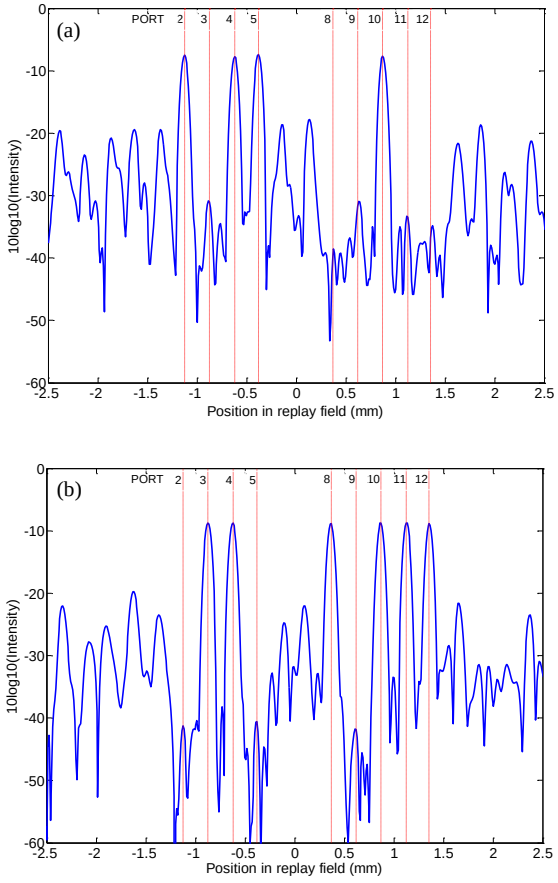

Fig. 5 *Theoretical GSSA algorithm replay fields when multi-casting to (a) Four ports. (b) Six ports. These plots were arbitrarily chosen from the hologram sets described in Table 2. Dashed lines show port positions.*

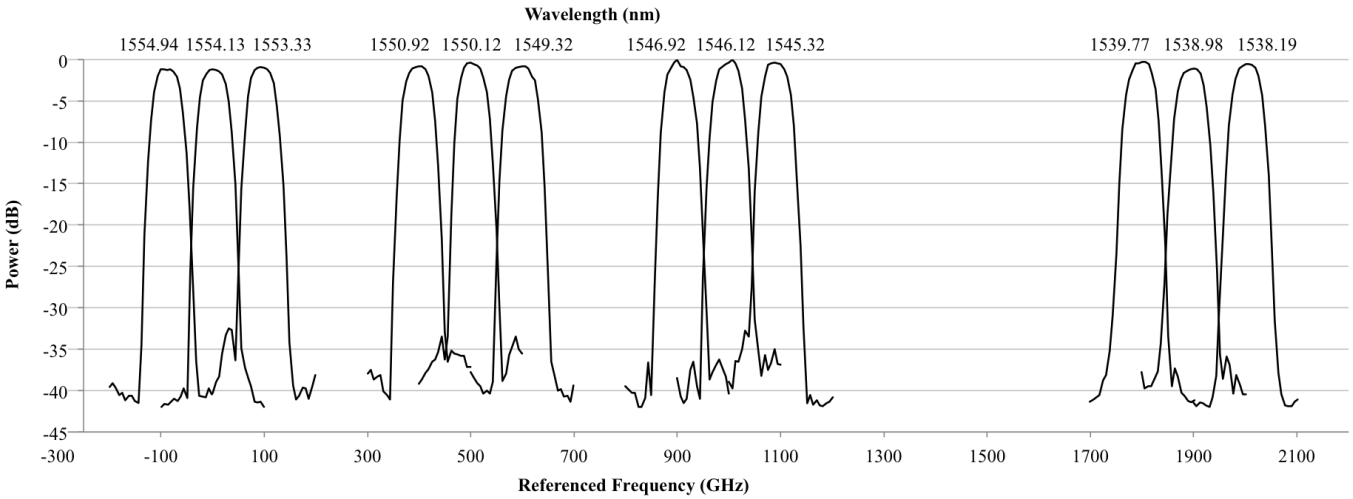

Fig. 7 *Measured passband at 12 ITU grid frequencies (100 GHz channel separation)*

III. Experimental Results

A. Single Port Deflection (100 GHz)

The experimental dependence of insertion loss on port position at a wavelength of 1554.13 nm is plotted in Fig. 6 alongside the theoretically predicted value, which accounts for fixed losses, aberrations, and grating efficiency roll-off. The latter factor includes the effect of spatial and phase quantization, and dead space [27]. The observed discrepancy between the two curves is primarily due to aberrations introduced by system misalignment, which cause the insertion loss to be asymmetric (section II.C), and a roll-off in diffraction efficiency due to the edge effect, where the voltage applied to one pixel affects its nearest neighbors. The effect is most pronounced where the phase drops from 2π to 0 radians, referred to as fly-back regions. Thus, as the period is reduced, the relative influence of this region increases [28, 30].

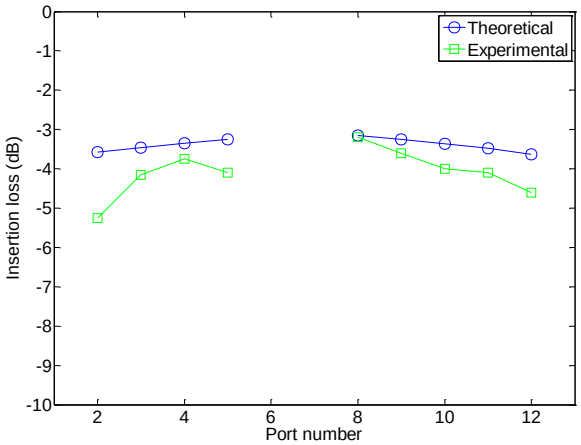

Fig. 6 *Theoretical and measured insertion loss for single port deflection at 1554.13nm.*

Crosstalk performance at 1554.13nm is summarized in Table 3, with columns giving the measured crosstalk at all ports when deflecting to a specific intended port. For clarity, each table entry is referenced to the minimum insertion loss of the switch (port 8 in Fig. 6). The measured crosstalk has an average value of -34.5 dB, and a maximum value of -21 dB. In general high crosstalk loss values occur for the +2 order and the -1 order of each hologram pattern. The +2 order crosstalk power is primarily due to reflection of the +1 signal order from the imperfect anti-reflection coated coverplate used (0.2 %), and the ITO layer. This reflected light is re-diffracted by the blazed grating into the same direction as the +2 order. Crosstalk at the -1 order positions is primarily due to the fly-back region, whilst the systematic occurrence of high crosstalk at ports immediate to the right and left of the signal beam is due to overspill of the light into neighboring lenslets caused by system misalignment and aberrations. The crosstalk between neighboring sub-holograms, defined as the amount of light incident on sub-hologram p that overspills onto, and is diffracted by sub-holograms p+1 and p-1, was also measured. At a wavelength of 1554.13nm, we obtain crosstalk values of –39.5 dB and –41 dB.

TABLE 3
Switch Crosstalk Matrix At 1554.13nm

	Intended port								
Port	2	3	4	5	8	9	10	11	12
2		-27.5	-40.5	-37.5	-38.5	-38.5	-43.5	-23.5	-24.0
3	-35.5		-26.9	-34.5	-39.7	-27.8	-27.5	-24.3	-44.5
4	-39.0	-34.9		-26.3	-36.0	-24.8	-28.5	-42.9	-34.5
5	-38.6	-31.2	-34.9		-21.0	-24.5	-41.3	-40.5	-38.8
8	-33.3	-33.2	-32.9	-21.1		-25.7	-33.2	-32.4	-33.1
9	-37.5	-36.3	-34.5	-27.0	-31.5		-25.8	-39.0	-37.7
10	-43.6	-27.0	-30.0	-39.5	-29.9	-35.1		-26.7	-36.7
11	-36.0	-25.8	-48.0	-30.8	-33.7	-34.0	-38.4		-27.2
12	-24.1	-46.9	-40.5	-42.7	-41.7	-33.7	-37.1	-34.6	

The passband of the switch was manually measured at twelve separate WDM frequencies using a tunable laser, with a typical value of 25-30 GHz for a -0.5 dB roll-off in insertion loss (Fig. 7). It should be noted that this experimental switch was not optimized for passband. In future we plan to address this by using techniques such as increasing the value of Q.

B. Dynamic Single Port Data Tests (100 GHz)

To test the operation of the switch with real data, a bit error rate (BER) test was performed with 100 GHz channel spacing, $\lambda = 1554.13$ nm, and a data rate of 10 Gbit/sec. The resulting eye diagrams for single port deflections to ports 4, 5, 8, and 9 are shown in Fig. 8 as a representative illustration of performance. In the case of single port deflection, the noise penalty of the switch is typically <0.5 dB, within the measurement limits of the test system. We can therefore conclude that the LCOS SLM introduces no measurable noise when displaying blazed gratings. Note that, due to equipment availability, not all the BER plots were taken at the same time. However, the noise penalty data was taken in consecutive measurements in a short period of time with the same pattern generation settings.

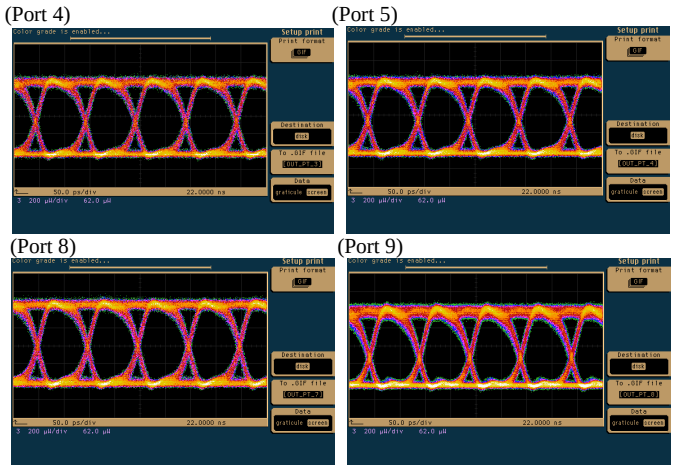

Fig. 8 Set of four eye diagrams taken at 10 Gbit/sec when a single signal is deflected to ports 4, 5, 8, and 9 ($\lambda = 1554.13$ nm).

C. Multi-casting (200 GHz)

A theoretical simulation of hologram performance covering all possible fan-out configurations was presented in section II.C using the actual switch and LCOS SLM parameters. The results presented in Table 2 show that this algorithm can theoretically minimize signal non-uniformity whilst maximizing SXR, although with a pattern dependent variation in diffraction efficiency. However, for this research paper we were also interested in experimentally testing the algorithm with respect to φ_{LIMIT}, whether a restriction in phase discontinuity in the SA optimization step can improve hologram performance. In addition, we also wanted to test the dynamic data performance (BER) of the switch when a multi-casting hologram was displayed. Thus, a series of holograms that deflected light to ports 2 and 3 whilst suppressing light to all other signal ports were designed. For these tests, the switch was configured such that best operation at 200 GHz channel spacing would be obtained (pitch between sub-holograms of 14Δ). Following from the work of Pernick [19], the results presented here will be equally valid for a switch operating with 100 GHz or 50 GHz channel spacing, as the diffracted power spectrum depends only on the phase profile in the y-direction, not on the width of the beam in the x-direction.

A range of φ_{LIMIT} values were used, with twenty holograms optimized for each value with the merit function adjusted to minimize non-uniformity between the two signal beams. Due to the probabilistic nature associated with the GSSA routine, the twenty optimized holograms generate slightly different replay fields. Thus, for each φ_{LIMIT} values we always choose the hologram that gave the lowest signal non-uniformity, as opposed to maximizing diffraction efficiency or SXR. For example, when we ran 20 optimizations for $\varphi_{LIMIT} = 2\pi$, the theoretical non-uniformity varied from 0.1 % to 0.4 %, whilst the associated SXR and diffraction efficiency varied from -43.2±7.3 dB and 38±1 % respectively. Using our design metric we choose the lowest non-uniformity of 0.1 %, which has an associated SXR of -36.5 dB. In future work we will determine a more effective way of choosing the best overall hologram.

Figure 9 shows the theoretical and measured dependence of overall diffraction efficiency on φ_{LIMIT} based on the set of measured holograms chosen using our minimum signal non-uniformity metric. Both curves follow similar trends; the diffraction efficiency gradually increases as the phase limit value is decreased until we hit a turning point at ~1.0 radians, at which point it rapidly increases towards the same value as for the single step GS algorithm (insertion loss of -3.96 dB).

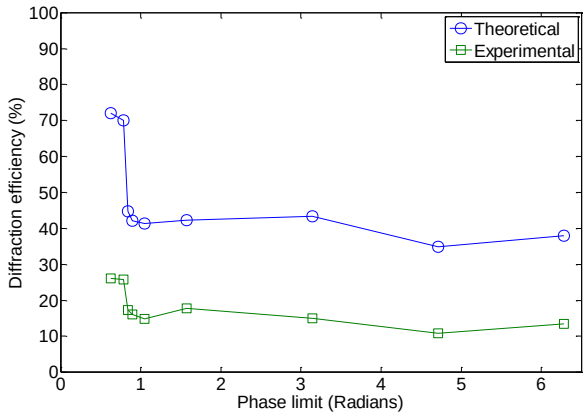

Fig. 9 *Theoretical and experimental dependence of diffraction efficiency on phase limit when multi-casting to two ports.*

Figure 10 shows that the corresponding theoretical and measured SXR as φ_{LIMIT} is reduced with the theoretical crosstalk suppression reducing gradually from approximately -38 dB to -48 dB until we reach the same turning point value of $\varphi_{LIMIT} < 1.0$ radians evident in Fig. 9. Thereafter the crosstalk rapidly increases to the Gerchberg-Saxton crosstalk value of -9.2 dB.

Experimentally we observe a similar trend, wherein the crosstalk suppression improves as φ_{LIMIT} is reduced from 2π to 1.0radians. In practice it is reduced from -17.4 dB to -20.8 dB. However, it is evident that the crosstalk improvement as a function of φ_{LIMIT} is also related to the algorithm and the merit function restrictions as opposed to any reduction in the edge effect due to limiting phase changes during the SA iterations as the two curves, although offset, have similar trends.

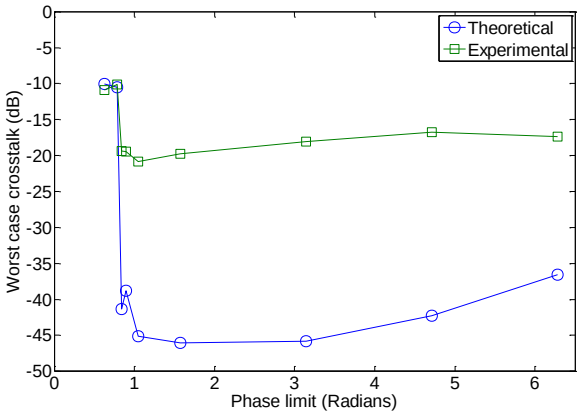

Fig. 10 Theoretical and experimental worst case crosstalk as a function of phase limit.

It was found that the non-uniformity of the optimized holograms can be reduced to <0.1 % by increasing the value of γ_u in equation 4. However, experimentally we still observed larger non-uniformities. This could be due to two factors. Firstly the theoretical phase response is not being faithfully reproduced due to the edge effect and phase flicker. Secondly, as the optimization algorithm employs a Gaussian apodization function to represent the actual beam, alignment errors could cause the beam to be off-centre or have an incorrect beam radius, which would lead to errors in the replay field.

Experimentally the worst case crosstalk suppression is within the same range as that obtained when displaying blazed gratings (-20 to -25 dB). We believe that improvements in both single port deflection and multi-casting performance can be obtained by using a better anti-reflection coated coverplate on the SLM, taking into account the non-uniform cell thickness when converting the ideal hologram phase levels to pixel voltages and by taking into account the pixel edge effect during hologram design [28, 30]. The use of a LCOS SLM with low phase flicker, defined as temporal variations in phase due to the addressing scheme [31], may also further improve performance.

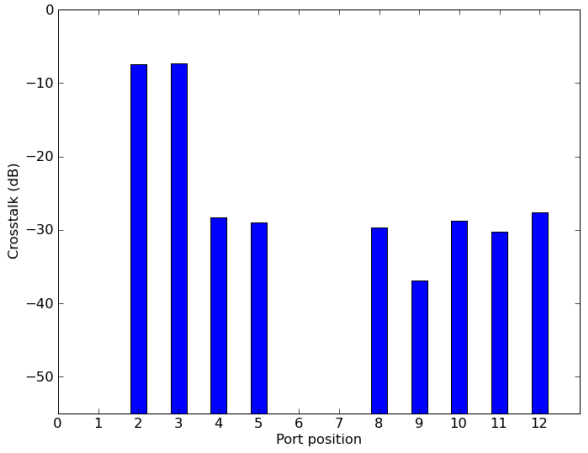

Fig. 11 Measured signal and crosstalk powers when deflecting to ports 2 and 3 in the switch.

Based on the measured data for our minimum non-uniformity metric, the best hologram in terms of crosstalk suppression and efficiency occurs when the phase limit value is set at 1.0 radian. The measured insertion loss (normalised to the power diffracted to a single port by a blazed grating) is plotted in Fig. 11. Maximum crosstalk suppression with respect to the average signal beam power is 19.4 dB, very similar to the blazed grating performance. The insertion loss is -7.6 dB (compared to our design value of -4.95 dB), and the uniformity between signals is ±0.6 %.

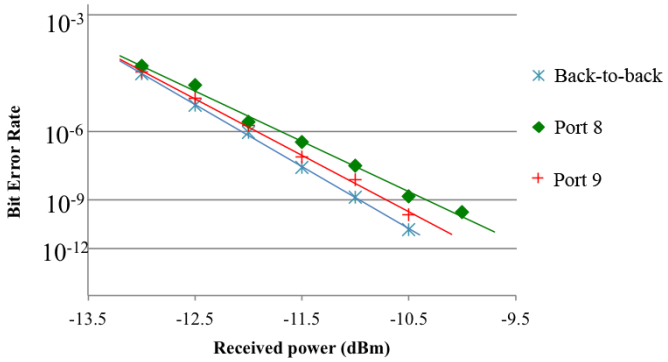

Fig. 12 *Noise penalty when multi-casting equal power to ports 8 and 9.*

Figure 12 shows the bit error rate noise penalty curves at 100 GHz/10 Gbit/s when the system was configured to multi-cast equal power to ports 8 and 9. In this case only the GS algorithm was used to design the hologram as we had not yet developed the GSSA algorithm. The curves for both signal beams and for the back-to-back measurement are plotted. The slight discrepancy between the two curves for the signal beams could be due to either a greater imbalance in optical power routed to the signal ports, or a higher sensitivity of these more complex holograms to phase flicker.

IV. Conclusion

A multi-functional LCOS based wavelength selective switch was developed and tested with constant power signals at 100 GHz and 200 GHz, and with dynamic data at 100 GHz/10 Gbit/s. The switch can deflect WDM signals to a specific output port using a blazed grating with a loss <-5.5 dB a worst-case crosstalk < -22 dB, and with a typical -0.5 dB passband of 25-30 GHz.

Our research shows that multi-casting sub-holograms can be designed using a two-step algorithm; a first step that optimizes the core hologram with a Gerchberg-Saxon routine, and a second step that uses a simulated annealing routine. We optimized holograms for all possible fan-out patterns with equal power weighting and show that, in all cases, the signal non-uniformity is < 3%, the crosstalk < -35dB, and the diffraction efficiency > 40%. It was also found that there is a pattern dependent variation in signal diffraction efficiency within a particular hologram sub-set. In future work we plan to optimize the merit function and investigate the role of spatial and phase quantization with the aim of minimizing this efficiency variation

Experimental tests of equal power deflection to two ports result in an insertion loss of -7.6 dB normalized to single port deflection by a blazed grating, a uniformity of ±0.6 %, and a worst-case crosstalk with respect to the average signal beam power of -19.4 dB. However, it is believed that further enhancement in performance can be obtained by including the edge effect in the hologram design, using an SLM with a low phase flicker, and compensating for LCOS SLM imperfections, such as cell thickness non-uniformity, and the finite reflectivity of the front cover plate and ITO layer.

Dynamic data measurements at 10 Gbit/s were performed for both single port deflection and multi-casting. For single port deflection the switch has no measurable effect on bit error rate. When multi-casting to two ports with equal power, we observe a slightly larger deviation from the back-to-back measurement, which may be due to the higher sensitivity of a complex phase hologram to phase flicker.

ACKNOWLEDGMENT

This work was supported by the Cambridge Integrated Knowledge Centre (CIKC), by the UK Engineering and Physical Sciences Research Council (EPSRC) platform grant (Liquid crystal photonics), by the Research Council UK (RCUK) Global Uncertainties program, and by the follow on fund (ACCESS project).

REFERENCES

[1] **M. Sharma, P. Hansen, B. Nayer, and P. Wigley, "Next-generation ROADM technologies and architecture", Photonics West 2012, Proc. Of SPIE Vol. 8283, 828309-1 (2012).**

[2] **Wavelength-selective switches for ROADM applications", T. A. Strasser, and J. L. Wagener, IEEE Journal of Selected Topics in Quantum Elect. 16, 1150-1157 (2010).**

[3] **D. M. Marom, D. T. Neilson, D. S. Greywall, C. S. Pai, N. R. Basavanhally, V.A. Aksyuk, D. O. López, F. Pardo, M. E. Simon, Y. Low, P. Kolodner, and C. A. Bolle, "Wavelength-selective 1×K switches using free-space optics and MEMs micromirrors", J. Lightwave Techn. 23(4) 1620-1630 92005).**

[4] **M. C. Wu, O. Solgaard, and J. E. Ford, "Optical MEMS for lightwave communication", J. Lightwave Technol. 24, 4433-4454 (2006).**

[5] **S. Frisken, G. Baxter G, D. Abakoumov, H. Zhou, I. Clark, and S. Poole, "Flexible and grid-less wavelength selective switch using LCOS technology", Proc. Optical Fiber Communication Conference (OFC), paper OTuM3 (2011).**

[6] **N. K. Fontaine, R. Ryt, and D.T. Neilson, "N×M wavelength selective crossconnect with flexible passbands", Proc. Optical Fiber Communication Conference (OFC), Post deadline paper PDP5B.2 (2012).**

[7] **O. Gerstel, M. Jinno, A. Lord, S. J. Ben Yoo, "Elastic optical networking: a new dawn for the optical layer", IEEE Comm. Mag., 50, S12-S20 (2012).**

[8] **M. Johansson, S. Hård, B. Robertson, I. Manolis, T. Wilkinson, and W. Crossland, "Adaptive beam steering implemented in a ferroelectric liquid crystal spatial-light-modulator free-space, fiber-optic switch, Appl. Opt., 41, 23, 4904-4911 (2002).**

[9] **A. Kirk and T. Hall, "Design of binary computer generated simulated annealing: coding density and reconstruction error", Opt. Commun. 94, 491-496 (1992).**

[10] **M. A. Sedowitz, J. P. Allebach, and D. W. Sweeny, "Synthesis of digital holograms by direct binary search", Appl. Opt. 26, 2788-2798 (1987).**

[11] **R. W. Gerchberg and W. O. Saxton, "A practical algorithm for the determination of the phase from image and diffraction plane pictures", Optik 35, 227-246 (1972).**

[12] **S. Frisken, H. Zhou, D. Abakoumov, G. Baxter, S. Poole, H. Ereifej, and P. Hallemeier, "High performance 'drop and continue' functionality in a wavelength selective switch", OFC 2006, PDP14 (2006).**

[13] **J. Schröder, M. A. F. Roelens, L. B. Du, A. J. Lowery, S. Frisken, and B. J. Eggleton, "An optical FPGA: Reconfigurable multi-spectral pulse-shaping for linear optical processing", Opt. Express, 21, 690-697 (2013).**

[14] **J. S. Liu, N. Collings, W. A. Crossland, D. P. Chu, A. Waddie, and M. R. Taghhizadeh, "Simulation and experiment on generation of an arbitrary array of intense spots by a tiled hologram", J. Optics 12, 085402 (2010).**

[15] **F. Zhang, N. Collings, J. J. Zhong, and W. A. Crossland, "Design of a free-space interconnection switch", Technical Digest of EOS Topical Meeting on Optics in Computing, pp. 55-56, Engelberg, Switzerland (2004).**

[16] **T. A. Nguyen, J. W. An, J. K. Choi, and N. Kim, "A hybrid algorithm to reduce the computation time of genetic algorithm for designing binary phase holograms", J. Opt. Soc. Korea, 7, pp. 264-268 (2003).**

[17] **Z. Zhang, A. M. Jeziorska-Chapman, N. Collings, M. Pivenko, J. Moore, B. Crossland, D. P. Chu, and B. Milne, "High quality assembly of phase-only liquid crystal on silicon (LCOS) devices", IEEE J. Display Techn., 7, 120-126 (2011).**

[18] **A. Georgiou, J. Beeckman, and K. Neyts, "Multicasting optical interconnects using liquid crystal over silicon devices", J. Opt. Soc. Am. A, 28, 363-372 (2011).**

[19] **B. J. Pernick, "Optical systems for combined 1-D image-orthogonal Fourier transform processing", Appl. Opt. 19, 754-760 (1980).**

[20] **M. A. F. Roelens, S. Frisken, J. A. Bolger, D. Abakoumov, G. Baxter, S. Poole, B. J. Eggleton, "Dispersion trimming in a reconfigurable wavelength selective switch", J. Lightwave Tech., 26, 73-76 (2080).**

[21] **LightSmyth Technologies, http://www.lightsmyth.com/**

[22] **J. R. Moore, N. Collings, W. A. Crossland, A. B. Davey, M. Evans, A. M. Jeziorska, M. Komarčević, R. J. Parker, T. D. Wilkinson, and H. Xu, "The silicon backplane design for an LCOS polarization-insensitive phase hologram SLM", IEEE Photonics Techn. Lett, 20, 60-62 (2008).**

[23] **UK Patent application GB1201190.4.**

[24] **C. Pulikkaseril, L. A. Stewart, M. A. F. Roelens. G. W. Baxter, S. Poole, and S. Frisken, "Spectral modeling of channel band shapes in wavelength selective switches", Optics Express, 19, 8458-8469 (2011).**

[25] **"Electromagnetic Theory of Gratings", R. Petit, ed., Springer-Verlag, Berlin (1980).**

[26] **Radiant Zemax, http://www.radiantzemax.com/**

[27] **D. G. Leyva, B. Robertson, C. J. Henderson, T. D. Wilkinson, A. C. O'Brien, and G. Faulkner, "Cross-talk analysis in a telecentric adaptive free-space optical relay based on a spatial light modulator", Appl. Opt. 45, 63-75 (2006).J. E. Stockley, D. Subacius, and S. A. Serati, "Influence of the inter-pixel region in liquid crystal diffraction gratings", in Liquid Crystal Materials, Devices, and Applications VII, R. Shashidhar ed., Proc. SPIE Vol. 3635, 127-136 (1999).**

[28] **A. G. Georgiou, M. Komarcevic, T. D. Wilkinson, and W. A. Crossland "Hologram optimization using liquid crystal modeling," Mol. Cryst. Liq. Cryst., 434, 183–198 (2005).**

[29] **R. E. Wagner and W. J. Tomlinson, "Coupling efficiency of optics in single-mode fiber components", Appl. Opt, 21, 2671-2688 (1982)**

[30] **M. Persson, D. Engström, and M. Goksör, "Reducing the effect of pixel crosstalk in phase only spatial light modulators", Optics Express, 20, 22334-22343 (2012).**

[31] **Boulder Nonlinear Systems, http://www.bnonlinear.com/**

Authors' biography not available at the time of publication.